Creep Deformation of Ice-Rich Silty Permafrost Under the Interactive Effects of Solid Fraction, Temperature, and Axial Stress

Ziyi Wang[*1]; Ming Xiao[1]; Matthew Bray[2]; Margaret M. Darrow[3]; Dmitry Nicolsky[4]; Xiaohang Ji[1]

[1]Department of Civil and Environmental Engineering, The Pennsylvania State University, University Park, PA 16802, United States of America.

[2]Institute of Northern Engineering, University of Alaska Fairbanks, Fairbanks, AK 99775-5900, United States of America.

[3]Department of Civil, Geological, and Environmental Engineering, University of Alaska Fairbanks, Fairbanks, AK 99775-5900, United States of America.

[4]Geophysical Institute, University of Alaska Fairbanks, Fairbanks, AK 99775, United States of America.

November 19, 2024

This manuscript is a non-peer reviewed preprint submitted to EarthArXiv.

This manuscript has been submitted to the Journal of Geotechnical and Geoenvironmental Engineering for publication consideration. Future versions may contain different content.

[*]E-mail: ziyiwang@psu.edu (Corresponding author)

Abstract: Permafrost degradation influences permafrost's creep deformation and stability, posing challenges for existing and future civil infrastructure in cold regions. The secondary creep rate is the controlling parameter for the design of civil projects. Solid fraction, temperature, and axial stress may interactively affect creep deformation rate of ice-rich silty permafrost; yet their interactive effects are not well understood. In this study, field samples of relatively undisturbed permafrost from the upper 1.5 meters of the Arctic Coastal Plain near Utqiaġvik, Alaska were first retrieved and analyzed. We conducted constant stress creep tests, unconfined compression tests, and unfrozen water content tests to assess the mechanical and physical properties of the permafrost cores. From these tests, mathematical relationships between secondary creep rate and volumetric solid fraction, temperature, and axial stress were proposed based on Glen's flow law. Combining the experimental results and mathematical relationships, we quantitatively investigated the interactive effects of solid fraction, temperature, and axial stress on creep deformation. The research yields the following findings. (1) Increasing volumetric solid fraction can either increase or decrease permafrost creep rate depending on temperature and axial stress. (2) At lower temperatures and lower axial stresses, for example, -10℃ and 500 kPa, increasing volumetric solid fraction enhances permafrost's resistance to creep and decreases creep rate. (3) Increasing temperature increases unfrozen water content and diminishes the strengthening effect of increasing solid fraction. This diminishing effect caused by unfrozen water content is amplified at higher solid fractions. (4) At warmer temperatures near the melting point and higher axial stresses, for example, -2℃ and 1000 kPa, permafrost at higher volumetric solid fractions is more susceptible to creep deformation with an increased creep rate.

Keywords: permafrost, creep deformation, volumetric solid fraction, temperature, axial stress

Introduction

Permafrost is soil or rock that remains at or below 0℃ for at least two consecutive years. It is widely distributed in the high latitude regions and occupies 24% of the land area of the northern hemisphere (Anisimov and Nelson 1996). The top layer above the permafrost, which freezes in the winter and thaws in the summer, is the active layer. In Arctic regions, permafrost has historically provided a reliable foundation for civil infrastructure, with structures anchored into permafrost to withstand various loads (Nixon and McRoberts 1976; Clarke 2007; Hjort et al. 2022). Frozen soils, due to the ice content, exhibit time-dependent deformation that is categorized into three phases: primary, secondary, and tertiary creep. The design of civil infrastructure foundations in cold regions aims to minimize secondary creep rate, ensuring that accumulated deformation remains within the maximum allowable limits over the lifespan of the structure (McFadden 2001). Global climate change, however, is driving the warming of the Arctic at up to four times the rate of lower latitudes (Rantanen et al. 2022). As air temperatures in the Arctic increase over time, ground temperatures rise, driving near-surface permafrost degradation (Biskaborn et al. 2019; Wang et al. 2023a, b). The degradation of permafrost degrade the physical and mechanical properties, which in turn adversely affect the creep deformation and stability of permafrost.

The deformation of frozen soils has been extensively investigated for the last several decades (e.g., Vialov 1965; Ladanyi 1972; Sayles 1974a, b; Weaver and Morgenstern 1981; Zhu and Carbee 1984; Vyalov 1986; Shelman et al. 2014; Yang et al. 2015; Shastri et al. 2021; Wang et al. 2022; Schindler et al. 2023). The creep deformation of ice-rich frozen soils under deviatoric stress is governed by two key physical processes in ice: the creep rate decelerating process and the creep

rate accelerating process (Orth 1988). The creep rate decelerating process is dominated by the impeded dislocation of ice caused by soil particle inclusions (Schindler et al. 2023). The creep rate accelerating process is dominated by the formation and growth of microcracks within the ice matrix (Hooke et al. 1980; Morgenstern et al. 1980). Frozen soil achieves its peak creep resistance at the point of minimum creep rate (Schindler et al. 2023). The primary factors influencing the peak creep resistance include the volumetric fraction of solid or ice (Arenson et al. 2004), unfrozen water content (and therefore temperature and solute concentration) (Arenson and Springman 2005), the fabric or cryostructure (Bray et al. 2012), and the state of stress (Cudmani et al. 2022). Cryostructure is the pattern of ice inclusions within a frozen soil; it is closely associated with cryolithology and Quaternary depositional environments. In the laboratory, the minimum creep rate of ice and ice-rich frozen soil can be characterized using Glen's flow law (Glen 1955; Andersland and Ladanyi, 2003). This power law equation is expressed as:

$$\dot{\epsilon} = A\sigma^n \tag{1}$$

where $\dot{\epsilon}$ is the minimum strain rate, σ is the effective deviatoric stress, A is the fluidity parameter inversely related to the viscosity, and n is the stress exponent.

Unfrozen water content in permafrost increases substantially when the temperature increases within a few degrees of the melting point of ice. Unfrozen water reduces the creep resistance of permafrost by weakening the ice matrix and particle-particle interactions (Bray 2013; Moore, 2014). The presence of unfrozen water also influences deformation by directly facilitating the relative displacement between ice and soil grains. The effects of the solid or ice volume fractions and unfrozen water content on deformation of a frozen soil can be included in parameters A and n by means of empirical formulae (Ladanyi 1972; Duval 1977; Nixon and Lem 1984; Arenson and

Springman 2005); however, these studies did not quantitatively address the interactive effects of the primary variables (e.g., solid fraction volume, temperature and salinity, stress state) mentioned above. There is still disagreement on the effect of solid fraction on the creep deformation rate of ice-rich soil. Research in this field, including Ting et al. (1983) and Ladanyi and Morel (1990), has found that an increase in the volumetric solid fraction enhances the strength of frozen soil. The maximum strength is typically achieved when the soil reaches its highest density and the pores are completely filled with ice. Other research, however, suggested that an increase in the volumetric solid fraction may either have no effect or reduce the strength of a frozen soil (Swinzow 1962; Zhu and Carbee 1984). This contradiction may be attributed to variables such as stress state, temperature, and salinity (Cuffey and Paterson 2010). Moore (2014) highlighted the competition between the role of solid particles in impeding ice creep and the mitigating effects of unfrozen water at particle-ice interfaces. However, the interactive effects of volumetric solid fraction, temperature, and axial stress magnitude on the deformation of ice-rich silty permafrost are still not fully understood.

The objectives of this research are to quantitatively analyze the secondary creep rate of ice-rich silty permafrost and understand the influences of volumetric solid fraction, temperature, axial stress, and their interactive effects on permafrost's creep deformation. This paper first presents the cryostratigraphy of deposits from five boreholes on the Arctic coastal plain near Utqiaġvik, Alaska; then the paper assesses key physical properties—water content, frozen wet density, salinity, Atterberg limits, and particle size distribution—of selected permafrost cores; it finally discusses the interactive effects of volumetric solid fractions, temperature, and axial stress on the creep deformation of ice-rich silty permafrost. Through these objectives, this paper aims to

advance the understanding of the complex dynamics that govern the geomechanical behavior of ice-rich silty permafrost.

Field Testing and Geological History

Soil Sampling

The field sampling was conducted at five locations on the undisturbed permafrost tundra near Utqiaġvik, Alaska in August 2022. Figure 1 presents an aerial view of the tundra with the layouts of the five boreholes, labeled S1 (71.3231°N 156.6144°W), S2 (71.3244°N 156.6103°W), S3 (71.3264°N 156.5994°W), S4 (71.3294°N 156.5933°W), and S5 (71.3322°N 156.5842°W). A total of 562.1 cm of relatively undisturbed permafrost cores of 4.0 – 4.3 cm in diameter were obtained using a battery-powered auger. The active layer thickness of the permafrost tundra was 14 to 27.9 cm at the time of the sampling. The vegetated active layer was carefully removed at the borehole locations and set aside. Each permafrost core was wrapped in plastic film with aluminum foil and placed into a portable freezer with frozen gel packs to keep the samples frozen. All collected cores were kept at negative temperatures during the entire period of transportation to the lab. After coring, the vegetated active layer was carefully restored to its original position. The study sites are located within the Barrow quadrangle of the geological map of Alaska (Wilson et al. 2015). This region is primarily covered with Quaternary unconsolidated surficial deposits, consisting mainly of silty sand.

Cryostratigraphy of Deposits

Figure 2 depicts the cryostratigraphy of the primary surficial deposits at the study site. Soil types and cryostructure were identified through a combination of field and laboratory characterizations.

At location S1 (Figure 2a), the active layer thickness was 14 cm at the time of sampling. From 14 to 90 cm depth, the core was primarily dark brown clayey silt with gravel. Ice occurred occasionally as 1.3-cm thick lenticular ice lenses. From 90 cm to 103 cm, the soil was medium brown silty sand with sparse fine gravel and reticulate ice.

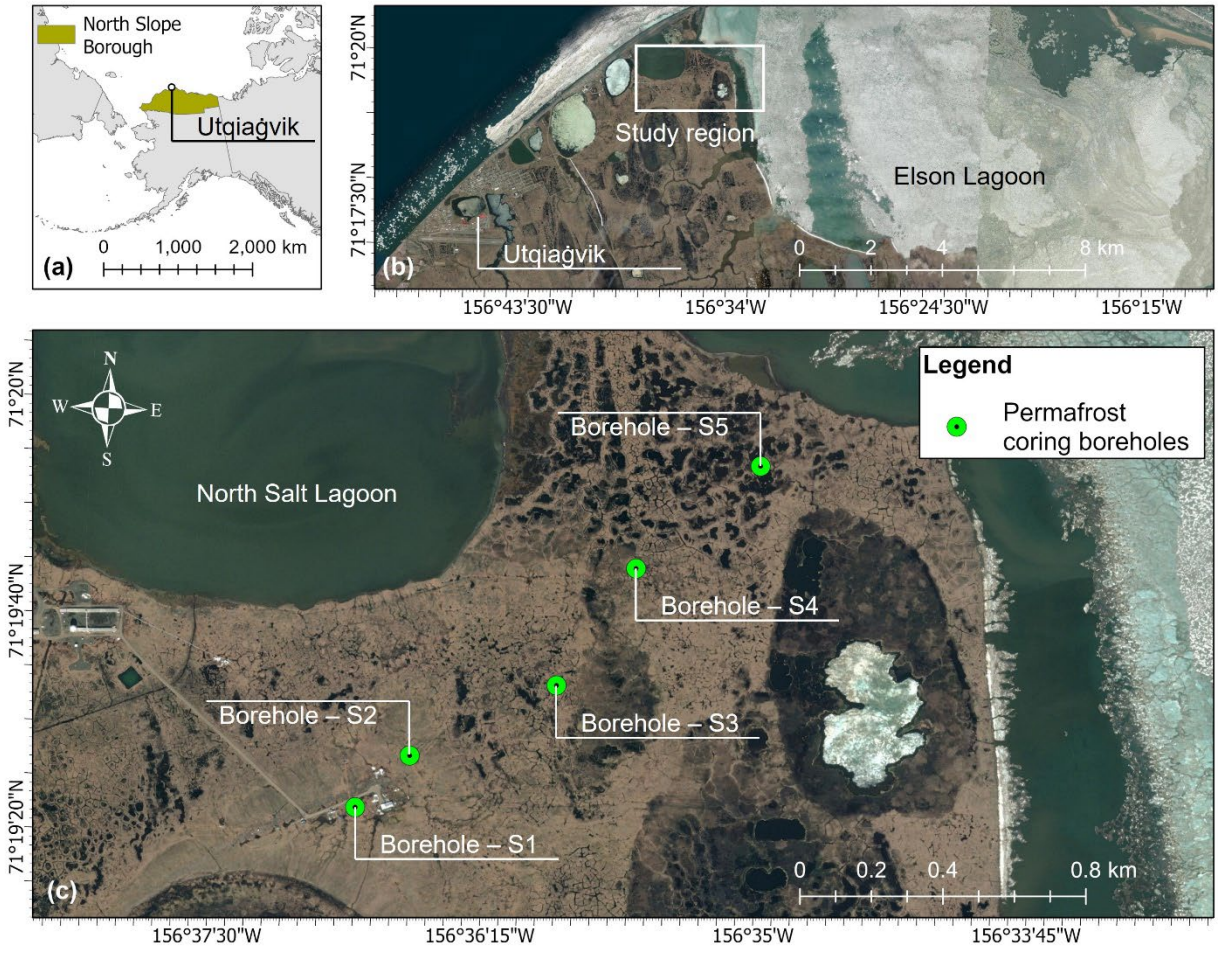

Figure 1. Field sampling map: (a) Utqiaġvik, North Slope Borough, Alaska (world borders data from World Countries Generalized, Esri); (b) study region; (c) aerial views of the five permafrost sampling locations (base map data from imagery copyright 2022 Maxar).

At location S2 (Figure 2b), the active layer thickness was 21.6 cm during sampling. The soil consisted of peat with woody fragments and roots from 21.6 cm to 36.8 cm. Ice was present as thin lenticular lenses and random ice lenses up to 0.1-cm thick. From 36.8 cm to 83.8 cm, the core

segments were primarily ice. From 83.8 cm to 147 cm, a general transition was observed from gray ice-rich sand to medium brown and slightly sandy silt with sparse fine gravel intermixed with ice zones. From 152 cm to 170 cm, the soil was brown silty sand with sparse fine gravel and contained only pore ice.

At location S3 (Figure 2c), the active layer thickness was 20.3 cm. The soil was ice-rich and primarily composed of peat and silty sand. The sand was highly silty with sparse fine gravel. From 20.3 cm to 40.6 cm, the soil was peat to silty peat. Ice was present in an organic matrix above 30.5 cm; below 30.5 cm was primarily ice. From 40.6 cm to 66.0 cm, the subsurface was primarily ice. Below the ice layer, the soil was typically silty sand suspended within ice (i.e., ataxitic cryostructure). From 66.0 cm to 104.1 cm, the soil was medium brown silty sand. Below 104.1 cm, the soil was gray silty sand.

At location S4 (Figure 2d), the active layer thickness was 23.8 cm during sampling. Most of the sampled sections were ice-rich. The soil consisted of silty peat to silt from 23.8 cm to 45.7 cm depth, silty sand suspended within ice from 48.3 cm to 142.2 cm depth, and silty sand with fine gravel with decreasing ice content with depth from 132.1 cm.

At location S5 (Figure 2e), the active layer thickness was 27.9 cm. The soil was peat to silty peat from 27.9 cm to 50.8 cm depth with pore ice (above 41.9 cm) and visible vertical and horizontal ice lenses (below 41.9 cm). From 50.8 cm to 64.8 cm, the soil was intermixed peat and medium brown soil. Ice was present in the organic matrix. From 64.8 cm to 104.1 cm, the soil consisted of intermixed peat and medium brown silty sand suspended in ice (i.e., ataxitic cryostructure). Ice

and silt layers occurred from 104.1 cm to 140.7 cm. From 140.7 cm to 154.9 cm, the soil was medium brown silt with layered and reticulate ice lenses up to 0.3-cm thick, with several ice lenses up to 2-cm thick.

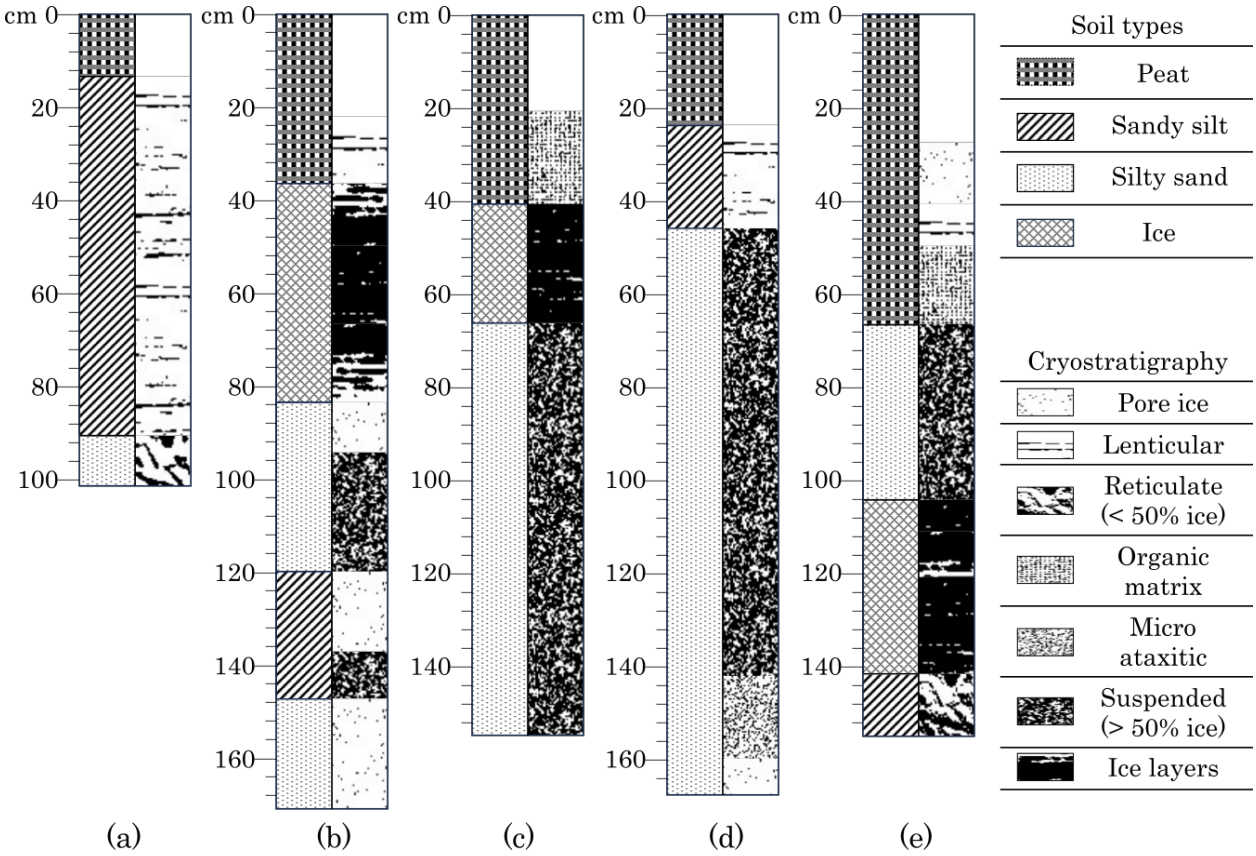

Figure 2. Cryostratigraphy of Arctic coastal plain deposits at the five sampling locations: (a) location S1; (b) location S2; (c) location S3; (d) location S4; and (e) location S5. The cryostructure classification system follows Kanevskiy et al. (2013).

Materials and Methods

Physical Properties and Sample Preparation

One objective of this study is to investigate the effect of solid fraction on the secondary creep rate of ice-rich silty permafrost. Factors including temperature and axial stress magnitude, which may interactively alter the effect of volumetric solid fraction, are also analyzed. Laboratory tests

included constant stress creep (CSC), unconfined compressive strength (UCS), and unfrozen water content (UWC) testing. The UCS and UWC test results were used to interpret the observed mechanisms of creep deformation under various stress, strain rate, and temperature conditions. We assessed physical properties such as total water content, Atterberg limits, grain size distribution, and salinity using the samples after the mechanical and unfrozen water content tests. Dry density, frozen volumetric solid fraction, thawed volumetric water content, and specific gravity were calculated based on phase relationships. These calculations assumed that the samples were fully saturated. Atterberg limit tests were repeatedly conducted for each sample until consistent and reproducible results were obtained (ASTM 2017). The grain size distributions of the samples were determined by conducting sieve analysis and hydrometer analysis, per ASTM C136 and ASTM D422, respectively.

The salinity of the permafrost was determined by measuring the concentration of soluble salts in the soil. The test method followed the standard ISO 11265:1994 (ISO 1994). A Milwaukee MW802 Pro Combo Meter was used for salinity measurements. The samples were first thawed. Then, a soil-water suspension was prepared by mixing 50 g of dry soil and 250 mL of distilled water. The suspension was soaked for an hour to let the salts dissolve completely. We calibrated the instrument with a standard solution of 1413 μS/cm. The measuring probe was rinsed with distilled water before taking each measurement in the suspension. Three salinity measurements were performed for each sample. The measured conductivity was converted to parts per thousand (ppt), which is approximately equivalent to g/L. Table 1 presents the basic physical properties of the tested samples. The sample number indicates the coring location (S2 to S5) and the sequential number of the sample from the top to the bottom depth in each borehole.

Table 1. Summary of physical properties of tested samples. ρ_{bf} is bulk frozen density, ρ_{dry} is dry density, w is gravimetric water content, θ_s is the volumetric solid fraction in the frozen state, θ_w is volumetric water content in the thawed state, LL is liquid limit, PI is plasticity index, and G_s is specific gravity.

Sample No.	Test	Depth (cm)	ρ_{bf} (g/cm^3)	ρ_{dry} (g/cm^3)	w (%)	θ_s (%)	θ_w (%)	Salinity (ppt)	LL	PI	G_s
S2-4	UWC	105-113	1.38	0.73	89.1	29.1	69.1	9.42	N/A	N/A	2.51
S2-5	UWC	130-137	1.22	0.84	45.1	58.6	39.3	15.24	N/A	N/A	1.43
S3-3	UWC	72-81	1.28	0.71	80.4	37.8	60.2	2.16	N/A	N/A	1.88
S3-4	UCS	81-89	1.45	0.91	59.0	41.3	56.6	4.04	26	2	2.21
S3-5*	UCS	92-100	1.57	1.05	50.1	42.8	55.0	5.45	26	1	2.44
S3-6*	UCS	114-122	1.38	0.73	89.5	28.9	69.3	4.10	20	1	2.52
S3-7	UWC	135-141	1.37	0.71	93.8	27.7	70.6	3.79	N/A	N/A	2.55
S3-7	UCS	146-155	1.23	0.49	149.7	19.6	79.0	1.77	22	1	2.52
S4-2*	CSC	52-61	1.16	0.43	171.5	20.1	78.5	0.84	26	3	2.13
S4-2	CSC	61-70	1.24	0.56	121.0	25.9	72.4	1.06	21	1	2.16
S4-3*	CSC	65-74	1.32	0.65	103.3	26.8	71.4	1.36	20	1	2.42
S4-3	UWC	74-81	1.39	0.70	98.4	24.8	73.5	2.22	N/A	N/A	2.83
S4-3	CSC	84-93	1.15	0.36	219.1	13.9	85.1	2.14	22	1	2.60
S4-4	CSC	99-108	1.28	0.53	140.6	18.4	80.3	1.06	27	3	2.89
S4-5*	UCS	124-132	1.26	0.52	143.2	19.1	79.6	1.02	33	4	2.72
S4-5	CSC	132-141	1.35	0.67	102.9	25.3	73.0	5.36	33	4	2.63
S4-6	UWC	147-156	1.82	1.38	31.7	52.2	45.6	8.03	N/A	N/A	2.65
S5-3*	UCS	64-72	1.05	0.27	295.9	14.4	84.5	0.46	27	3	1.84

* Indicates the specimens were also tested for UWC.

Selected permafrost cores for laboratory testing were uniform in both soil type and cryostructure. We chose samples with a minimum length-to-diameter ratio of 2:1 to reduce end effects on mechanical behavior. Samples with significant tapering and uneven diameters along their length were excluded from testing. The diameter of the selected samples varied between 4.0 to 4.5 cm. Figure 3 consists of photographs of the selected permafrost samples before the mechanical tests. The selected permafrost cores were ice-rich, with solid particles suspended in ice. The solid volume fraction, θ_s, of the samples in the mechanical tests ranged from 14% to 43%. Figure 4 illustrates the grain-size distributions of the selected samples for the laboratory tests, which were classified as ice-rich silty sand (SM). The comprehensive photographs of the retrieved samples from each borehole are shown in Table S1 in the supplementary materials.

Mechanical Tests – UCS and CSC

We tested six samples for UCS and six samples for CSC with stepped increase in stress; three samples were tested at -2°C and three at -10°C for both UCS and CSC testing. Figure 5 illustrates the test setup for these tests. The UCS tests were performed on electro-mechanical screw-driven load frames, at a strain rate of 0.6 per hour according to ASTM D7300. The loading frames were placed in a walk-in cold room maintained at room temperature of -5°C. Insulated chambers surrounded the loading pistons and frame. Within each chamber, a convection-driven heat exchanger was placed in series with an external cold bath to achieve a specific temperature and maintain chamber temperature stability of ± 0.03°C. The air temperature around the samples was monitored by four calibrated thermistors in close proximity to the sample. A latex membrane was placed around each sample to eliminate sublimation.

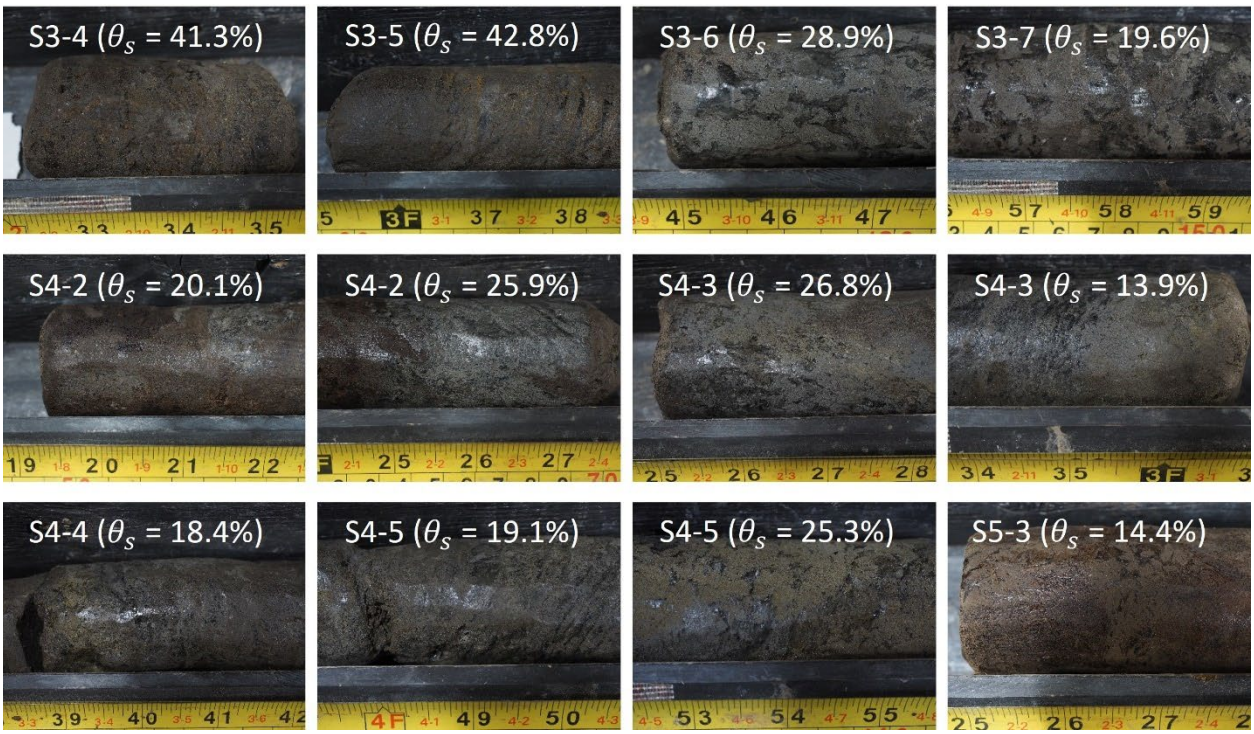

Figure 3. Selected permafrost cores for laboratory testing.

The CSC tests were conducted using an environmentally-equipped servo-control hydraulic load frame. Sample temperature was controlled by fitting a secondary insulated chamber within the main environmental chamber. The secondary chamber contained a convection-driven heat exchanger connected to an external refrigerated recirculating bath with temperature stability of 0.01°C. This temperature-control system maintained chamber temperature stability of ± 0.02°C. We monitored the sample temperature with four calibrated thermistors spaced around the sample. The average of these four temperatures were used as the temperature of the sample. A latex membrane was placed around each sample to eliminate sublimation. Prior to testing, all samples were given a minimum of 24 hours to equilibrate to a constant temperature.

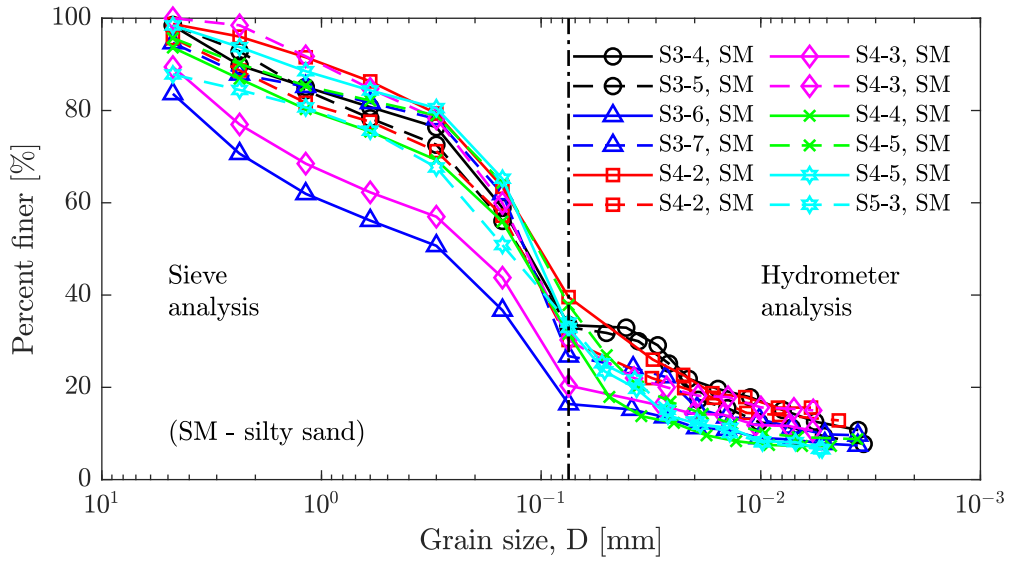

Figure 4. Grain-size distributions of tested samples.

During the CSC tests, the applied load was monitored and maintained within 4.5 N of the target load. Considering the increase in the sample's cross-sectional area due to deformation, which was assumed to be entirely plastic, the load was adjusted during the test to sustain a constant stress condition. This adjustment was made for every 0.1 cm of vertical deformation. After the UCS and

CSC tests, we photographed each sample and measured its total water contents. In the CSC tests, a minimum of four increasing stress steps were applied. Each stress level was typically maintained for four days unless tertiary creep occurred. During the CSC tests at -2°C, we applied four stress steps to three samples, with the deviatoric stresses set at 103.4, 172.4 (increased to 206.8 for S4-3), 275.8, and 344.7 kPa. For the CSC tests at -10°C, additional stress steps were conducted on sample S4-2 for a detailed creep analysis, with applied stresses of 172.4, 275.8, 413.7, 586.1, 792.9, 1103.2, and 1379.0 kPa. Based on creep response of S4-2, the stress steps were reduced to four for samples S4-3 and S4-5, with stresses of 586.1, 792.9, 1103.2, and 1379.0 kPa; however, only the first three steps were completed for S4-3 due to temperature control issues.

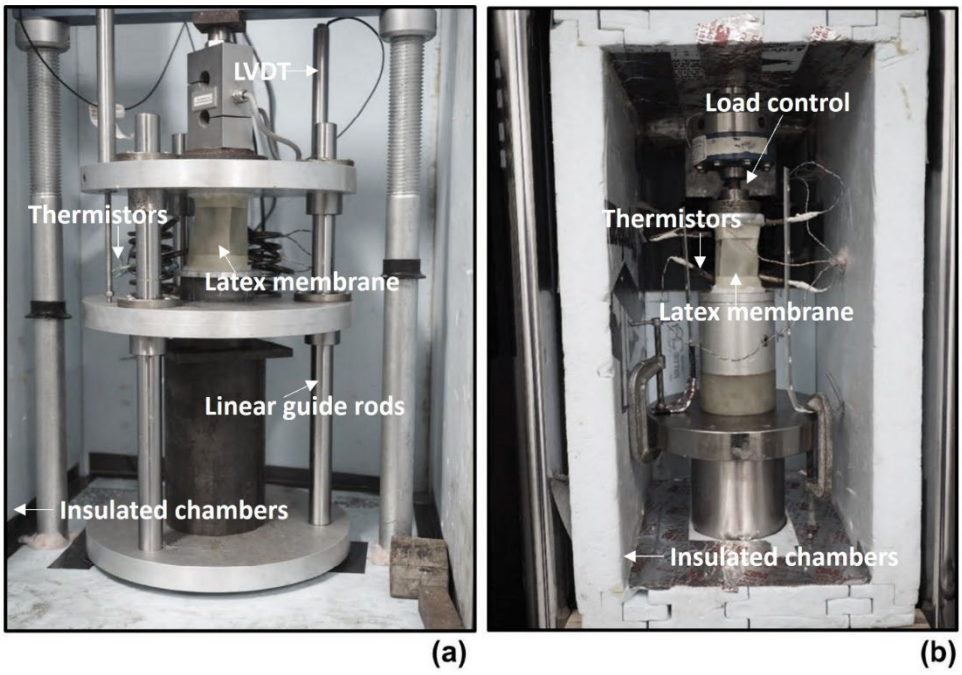

Figure 5. Test setup and sample placement: (a) UCS test and (b) CSC test.

Unfrozen Water Content (UWC) Tests

The UWC as a function of temperature for 12 samples was measured using a pulsed nuclear magnetic resonance (P-NMR) testing system. The P-NMR testing system included a modified

refrigerator for the testing environment. The P-NMR device, complete with a variable temperature probe, was placed inside the refrigerator within an insulated box to maintain the operating temperature of the magnet. Together with external refrigerated circulating baths, this setup precisely controlled the sample temperature. The samples for UWC measurements were cored with a 1.4-cm diameter hole saw, typically to a length of 4 cm. Then, the UWC was measured at -20, -10, -5, -3, -2, -1, -0.5, 5, and 10°C. After each change in temperature, samples were allowed to reach thermal equilibrium for 2 hours. We generally followed the normalization method (Kruse et al. 2018); however, when calculating the UWC, only the value of the free induction decay signal intensity determined at 10°C was used for the normalization reference value per soil type. The testing method had an accuracy of ± 2% gravimetric water content.

Statistical Analysis

Multilinear regression analysis was conducted to study the relationship between various predictors (e.g., volumetric solid fraction and temperature) and response variables. The mechanical tests were performed under relatively low salinity (below 5.5 ppt). We only considered the volumetric solid fraction and temperature in the analysis for mechanical properties. The response variables include parameters of Glen's flow law and parameters of UWC power law model (Anderson and Tice 1973). The power law model of UWC was used to interpret the mechanisms of creep deformation. To analyze the interactive effect of multiple predictors on the response variables, we conducted a second-order multilinear regression analysis with an interaction term. A basic equation with two predictors and an interaction term was first assumed:

$$Y = \beta_0 + \beta_1 x_1 + \beta_2 x_2 + \beta_3 x_1 x_2 \quad (2)$$

where Y is the response variable or predicted outcome, β_0, β_1, β_2, β_3 are the coefficients, and x_1 and x_2 represent the input variables or predictors. Given the potential for nonlinear relationships, predictors may be transformed into natural logarithmic scale to linearize their relationships with the response variables. The backward elimination process was followed for model building. First, we started with a full model with two predictors and an interactive term. A joint model utility F-test was performed to generate a P-value to assess whether any of the predictors provided significant information about the response variable. Partial F-tests were also performed to generate individual P-values to evaluate the strength of the association between the response variable and each predictor, including the interactive term. Then, at each step, a predictor was removed based on the partial F-tests when an individual P-value was higher than 0.005. A P-value equal to or below 0.005 indicated a statistically significant linear association between two parameters at a 99.5% confidence level. The effectiveness of the correlation was evaluated using the adjusted coefficient of determination (R^2) and the root-mean square error (RMSE) values. To develop an optimal description model, we adhered to three principles: 1) P-values less than 0.005, 2) the lowest possible RMSE, and 3) the highest adjusted R^2.

Results and Analyses

Time-dependent Deformation Behavior under the CSC Tests

Figure 6 depicts the creep behavior from the six stepped CSC tests. Figures 6a and 6b plot the axial strain and axial strain rate over time at -2℃; Figures 6c and 6d illustrate the progression of axial strain and axial strain rate over time at -10℃. As stepped stress increases, the typical creep behavior of frozen soil is observed: axial strain increases over time, and the strain rate initially decreases (in primary creep), reaches a minimum (in secondary creep), and then increases (in

tertiary creep). The stepped stress increase resulted in a jump in the strain rate. At low deviatoric stress levels, permafrost may remain in primary creep by the end of the loading stage, as indicated by not reaching a minimum or constant strain rate. The six permafrost samples all entered a tertiary creep within the tested stress range.

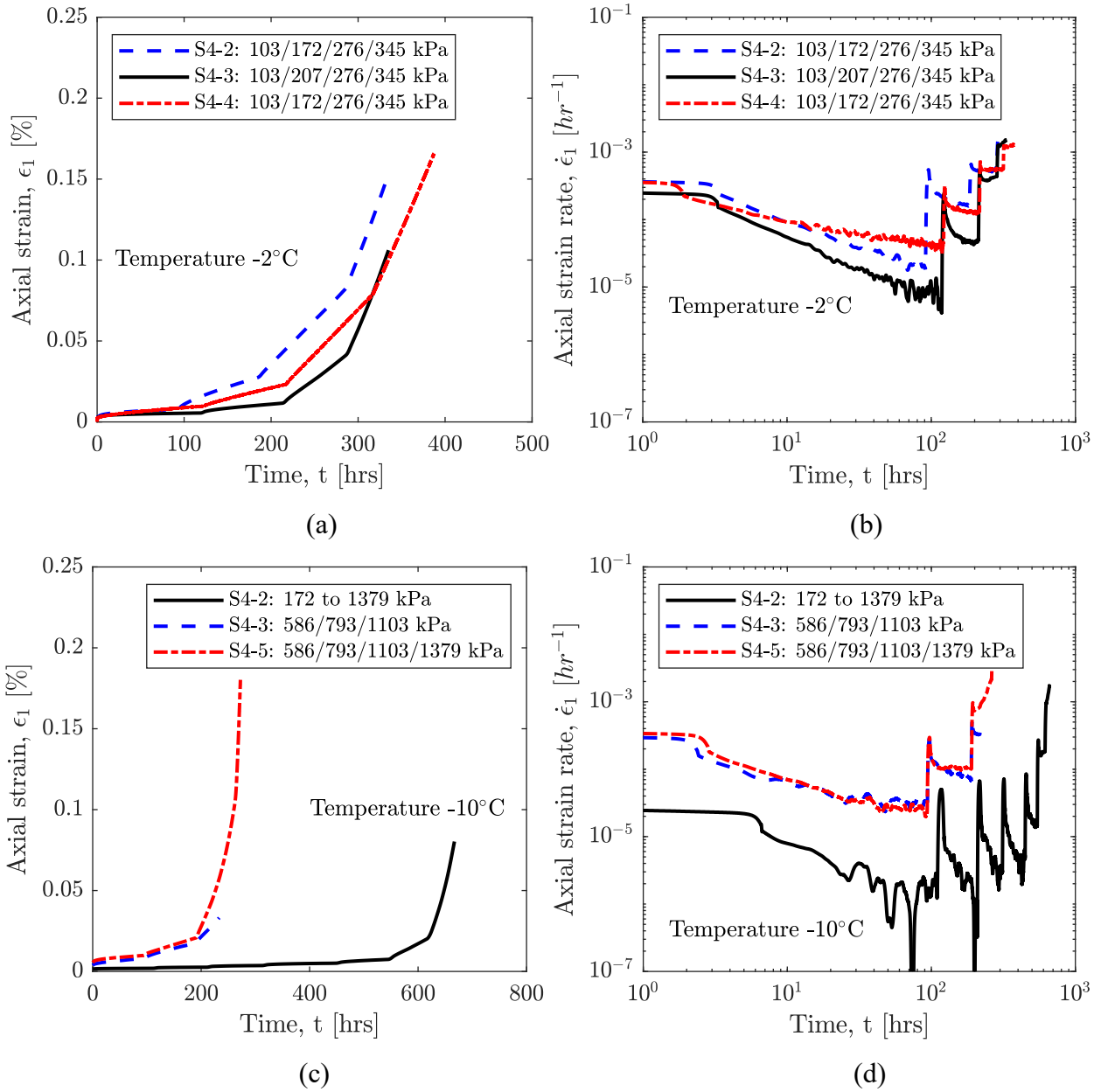

Figure 6. Creep behavior from stepped constant stress creep tests: (a) axial strain vs. time at -2℃; (b) axial strain rate vs. time at -2℃; (c) axial strain vs. time at -10℃; (d) axial strain rate vs. time at -10℃.

The samples exhibited lower axial strain rates at -10℃ compared to those at -2℃ under the same applied stresses. Specifically, sample S4-2 showed damped creep at -10℃ under 275.8 kPa, unlike the secondary creep or tertiary creep observed at -2℃. Damped creep is characterized by a continuously decreasing strain rate that theoretically eventually approaches zero. Moreover, the total axial strain during primary creep at -10℃ was significantly lower than that at -2℃ under the same deviatoric stress. Tertiary creep initiated at much higher stresses within the same testing period for the samples at -10℃ compared to those at -2℃. However, upon reaching a certain stress, the strain rate rapidly increased, leading to eventual failure.

Based on the results in Figure 6, the minimum strain rates at each stress stage were plotted in Figure 7, using the methodology summarized by Bray (2012). Using Glen's flow law, we determined the secondary creep parameters, A and n, by correlating axial stress (the applied deviatoric stress in each step of the CSC tests) with the minimum strain rate.

At -2℃, sample S4-4 with the lowest volumetric solid fraction (0.18) among the three samples exhibited the highest minimum strain rate during the secondary creep compared to the others; sample S4-3 with the highest volumetric solid fraction (0.27) showed the lowest minimum strain rate. At -10℃, analogously, sample S4-2 with the highest volumetric solid fraction (0.26) exhibited the lowest minimum strain rate among the three samples. These observations align with Ting's (1983) finding that within a certain stress range, solid particles can hinder creep deformation during the strain-hardening process. Thus, an increase in the volumetric solid fraction enhances the frozen soil's resistance to creep within the stress range of the tests.

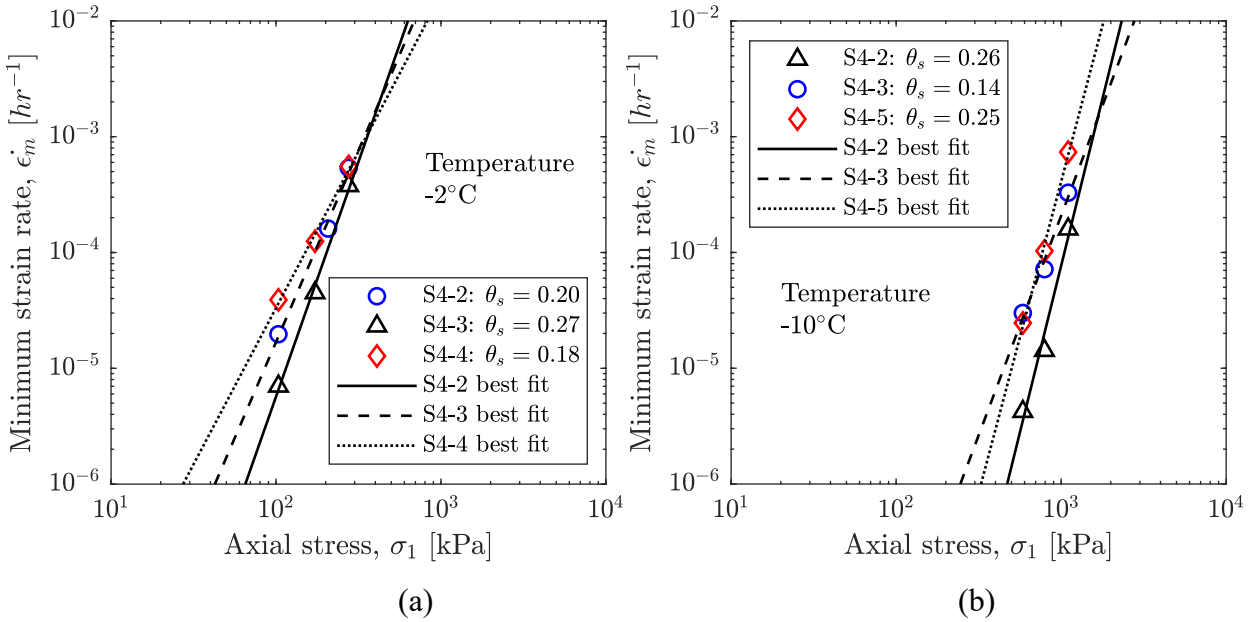

Figure 7. Glen's flow law of secondary creep rate: (a) at -2°C and (b) at -10°C.

Table 2 provides a summary of the parameters A, n, and R^2, using the test data in this study and the literature. The creep parameters have strong correlations with the experimental data, as indicated by R^2 ranging from 0.974 to 0.996. The values of A and n are used to establish relationships of volumetric solid fraction and temperature and to quantify the effects of solid fraction, temperature and axial stress on secondary creep rate.

Effect of Temperature and Solid Fraction on Secondary Creep Parameters

Data in this study were combined with the data in the literature to understand how volumetric solid fraction and temperature affect secondary creep parameters of ice-rich silty permafrost. Figure 8 presents a scatter plot of 29 data points and illustrates the relationships among A, n, solid fraction, and temperature. The temperature factor was defined as $1/(1+|T|)$ (Voytkovskiy 1960), where $|T|$ is the absolute value of temperature. The triangle and square data points represent the data from

previous studies on undisturbed ice-rich silty permafrost and remolded ice-rich frozen silt. (Bray 2012, 2013).

Table 2. Summary of the parameters of Glen's flow law for determining minimum strain rate.

Sample No.	Temperature (°C)	σ_{range} (kPa)	θ_s (%)	n	A (hr^{-1} kPa^{-n})	R^2	References
S4-2	-2	103 – 345	20.1	3.31	4.03E-12	0.996	Current study
S4-2	-10	172 – 1379	25.9	5.76	3.97E-22	0.974	
S4-3	-2	103 – 345	26.8	4.06	4.36E-14	0.994	
S4-3	-10	586 – 1103	13.9	3.79	8.60E-16	0.983	
S4-4	-2	103 – 345	18.4	2.70	1.32E-10	0.991	
S4-5	-10	586 – 1379	25.3	5.38	2.92E-20	0.996	
3, 4, 5, 12, 18	-1	159 – 311	24.4	4.17	4.88E-14	0.701	Bray (2012)
1, 2, 5, 12, 13, 14	-2	159 – 784	24.8	4.70	2.80E-16	0.822	
23	-0.77	31 – 1000	23.4	4.18	4.32E-14	0.955	Bray (2013)
24	-0.86	28 – 800	23.6	3.35	5.94E-12	0.986	
25	-2.78	247 – 1000	19.4	5.65	1.81E-19	0.998	
26	-0.77	58 – 800	24.6	4.38	5.04E-14	0.956	
27	-0.82	58 – 1000	24.2	3.99	3.78E-13	0.989	
28	-1.81	151 – 1000	27.2	6.38	1.61E-20	0.971	
28	-2.81	198 – 1400	27.2	6.37	5.72E-21	0.976	
29	-1.86	150 – 1400	23.9	4.53	1.40E-15	0.997	
29	-2.81	176 – 1500	23.9	4.39	2.19E-15	0.989	
30	-1.82	151 – 1500	25.8	4.78	2.73E-16	0.992	
49	-1.05	400-1196	40.3	5.15	8.57E-17	0.960	
50	-0.99	350-965	42.8	5.34	3.67E-17	0.997	
51	-1	400-983	42	5.43	2.21E-17	0.995	
52	-1.98	700-1613	43.2	7.11	2.55E-23	0.992	
53	-1.99	700-1648	45.9	7.19	1.61E-23	0.969	
54	-3.01	950-1903	40.2	7.8	3.74E-26	0.975	
55	-2.99	900-1700	42.2	8.39	5.26E-28	0.958	
60	-4.02	1100-2153	40.2	9.03	8.86E-31	0.982	
61	-4.01	1100-2371	38.7	8.27	2.19E-28	0.982	
62	-5.01	1400-2588	42.9	8.64	3.16E-30	0.991	
63	-5.01	1500-2778	40.1	7.22	3.04E-25	0.965	

σ_{range} indicates the stress range used for determining creep parameters A and n.

Figure 8a illustrates the regression surface for creep parameter A as modeled by the multilinear regression; parameter A is represented in logarithmic scale. Figure 8b presents the regression surface for creep parameter n. A decreases with an increase volumetric solid fraction. This decrease becomes more pronounced at lower sub-freezing temperatures, characterized by a faster decline in

parameter A with increasing volumetric solid fraction under these colder temperatures. The decrease of A indicates increased creep resistance with the enhancement of viscosity. A also increases with rising sub-freezing temperatures, with this effect being more pronounced at higher solid fractions. The creep parameter n increases with an increase in solid fraction, and this trend is more noticeable under colder temperature conditions. The increase in n indicates an increased nonlinear relationship between axial stress and minimum strain rate, wherein the minimum strain rate increases dramatically with higher axial stress. As the sub-freezing temperature increases, parameter n decreases, but this decrease is less marked at lower solid fractions. Theoretically, parameter n stabilizes at a constant value of 3 for polycrystalline ice with no solid fraction, irrespective of the sub-freezing temperature (Glen 1955; Morgenstern et al. 1980).

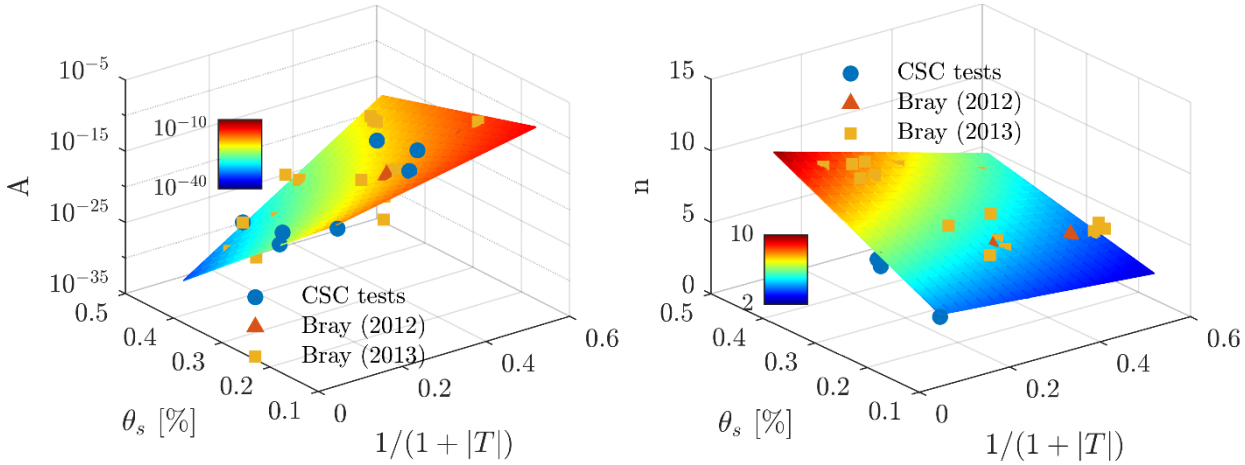

Figure 8. Multilinear regression analysis for creep parameters of ice-rich silty permafrost: (a) regression surface for creep parameter A; (b) regression surface for creep parameter n.

We established the relationship (Eq. 3) between creep parameter A and solid fraction and temperature by plotting $\ln A$ against $1/(1+|T|)$ and θ_s. Similarly, we established the relationship

(Eq. 4) between creep parameter n and $1/(1+|T|)$ and θ_s. Consequently, Glen's flow model (Eq. 1) of ice-rich silty permafrost as a function of solid fraction and temperature is expressed in Eq. 5.

$$\ln A = -14.1 - 154.1\theta_s + \frac{186.9}{1+|T|}\theta_s \tag{3}$$

$$n = 1.4 + 20.1\theta_s - \frac{19.6}{1+|T|}\theta_s \tag{4}$$

$$\dot{\epsilon}_m = \exp[-14.1 - 154.1\theta_s + \frac{186.9}{1+|T|}\theta_s]\,\sigma^{1.4+20.1\theta_s-\frac{19.6}{1+|T|}\theta_s}$$
$$0.15 \le \theta_s \le 0.45; -10℃ \le T \le -1℃ \tag{5}$$

A significant linear relationship exists between the interactive terms and the linearized creep parameters A and n, evidenced by individual P-value of 0.000. The regression analysis yielded adjusted R^2 values of 0.87 for parameter A and 0.83 for parameter n, with corresponding RMSE of 4.8 and 0.7, respectively. This semi-empirical model is developed based on experimental data with a volumetric solid fraction between 14% to 46% and temperature between -10℃ to -0.77℃. The ranges of the parameters represent typical ice-rich silty permafrost with near-surface ground temperature profiles in Northern Alaska.

Variations of Unfrozen Water Content (UWC)

Based on laboratory testing, unfrozen water content and temperature can be presented in the form of a simple power law (Anderson and Tice 1973; Bray 2013):

$$\theta_{n,u} = C\left(\frac{T}{T_0}\right)^b \tag{6}$$

where $\theta_{n,u}$ is the normalized volumetric unfrozen water content by the total volumetric water content, T_0 is the reference temperature of -1℃, and C and b are two experimentally-determined

parameters of the power law model. Table 3 summarizes the results of gravimetric UWC of the 12 permafrost samples as a function of temperature ranging from -20℃ to 10℃. As expected, the gravimetric UWC increases with rising sub-freezing temperatures and eventually approaches the total gravimetric water content, w, once the temperature exceeds 0℃.

Based on the results in Table 3, the volumetric UWC (θ_u) was calculated and normalized by total volumetric water content (θ_w) to have a range between 0 to 1. Using the power law model of UWC (Eq. 6), we determined the parameters, C and b, by correlating temperature with the normalized UWC. Figure 9 depicts the experimental results of normalized volumetric UWC of all samples as a function of sub-freezing temperature. The dashed lines represent the best-fit models. The power law models demonstrated a robust correlation with the experimental data, evidenced by R^2 values ranging between 0.969 to 0.998. The values of C and b are used to establish relationships between the volumetric solid fraction and salinity with the unfrozen water content and eventually to quantify the role of the unfrozen water in the creep deformation of permafrost.

Table 3. Unfrozen gravimetric water content (%) of the tested samples at different temperatures.

Temperature (℃)	S2-4	S2-5	S3-3	S3-5	S3-6	S3-7	S4-2	S4-3	S4-3	S4-5	S4-6	S5-3
-20.02	4.3	3.3	3.1	2.1	2.0	2.3	5.4	1.3	1.4	1.6	1.5	12.1
-10.02	6.1	5.8	3.9	2.6	2.5	3.6	5.9	2.4	1.3	3.1	2.4	12.1
-5.01	9.2	9.3	5.4	3.7	4.1	6.7	8.1	3.2	3.0	6.5	3.8	14.6
-3.03	13.6	13.4	5.9	4.8	5.2	8.4	8.5	4.2	4.2	7.9	5.3	19.3
-2.01	18.3	19.3	6.9	5.7	6.7	11.1	9.5	5.1	4	10.9	7.3	19.9
-1.05	35	37.9	9.1	9.5	11.9	17.3	11.9	6.6	6.5	14.6	13.8	24.9
-0.54	54.8	53.8	13.1	14.2	18.2	25.4	15	9.9	11	20.4	19.9	27.7
+9.98	75.1	80.9	66.7	51.8	67.9	105.7	185.6	83.3	83.6	147.1	26.1	525.7

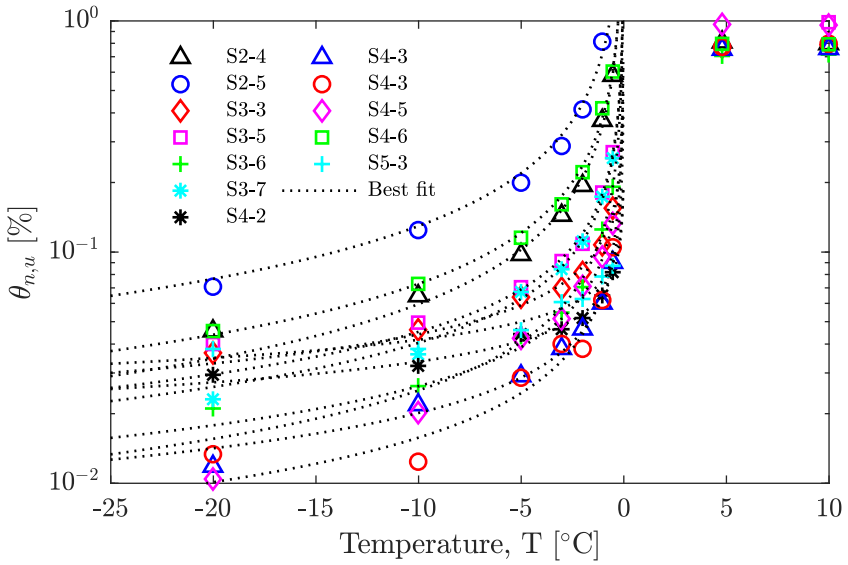

Figure 9. Relationship between normalized volumetric UWC ($\theta_{n,u}$) and temperature.

Effect of Salinity and Solid Fraction on the UWC Parameters

Solute concentration and finer solid fraction may increase unfrozen water content, subsequently reducing the strength and affecting the deformation properties of frozen soil (Anderson and Morgenstern 1973; Hivon and Sego 1990; Watanabe and Wake 2009; Chuvilin et al. 2022). Both solute concentration and solid fraction may influence the mechanisms of soil freezing point depression. The mechanisms of soil freezing point depression include capillarity in small pores, adsorption on mineral surfaces, and the presence of dissolved salts in pore water (Dou et al. 2016). In addition to freezing point depression, salinity and solid fraction may interactively influence the unfrozen water content by affecting thermal properties (Dash et al. 2006) and modifying the water retention capacity of soil (Konrad 1990).

The effects of salinity and the solid fraction on the parameters *C* and *b* of the UWC model were studied using multilinear regression analysis on the UWC tests data. Figure 10 illustrates the

variation of the power law parameters C and b with their corresponding solid fraction and salinity values.

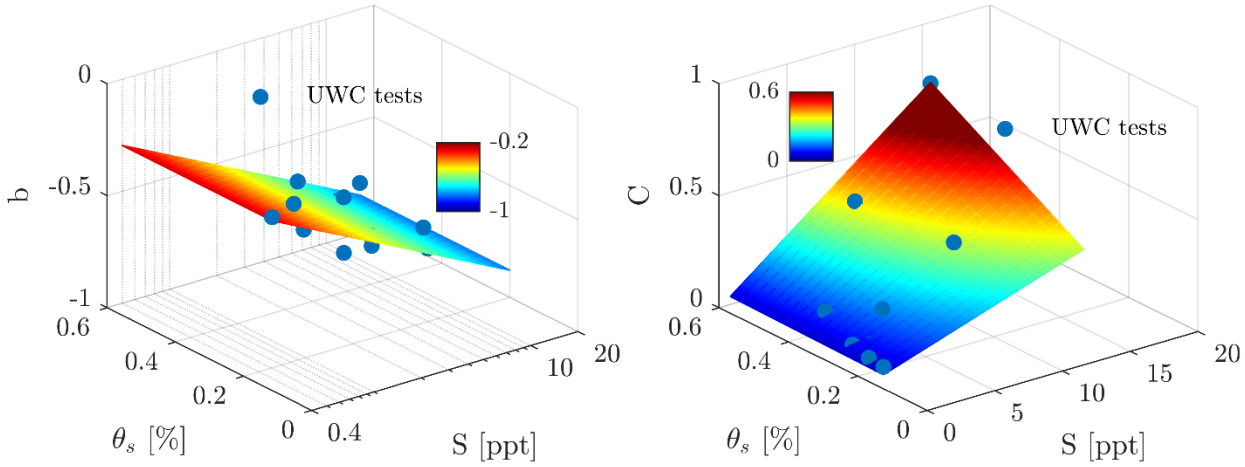

Figure 10. Multilinear regression analysis for UWC: (a) regression surface for power law parameter b; (b) regression surface for power law parameter C.

The UWC power law model and parameters b and C in relation to solid fraction and salinity are formulated in Eq. (7) to (9). In Eq. (7), salinity, S, is transformed to natural logarithmic scale to linearize the relationship, thereby improving the fit of the model.

$$b = -0.4 - 0.15 \ln S \tag{7}$$

$$C = 0.03 + 0.01S + 0.06S\theta_s \tag{8}$$

$$\theta_{u,n} = (0.03 + 0.01S + 0.06S\theta_s)T^{-0.40-0.15 \ln S}$$
$$0.15 \leq \theta_s \leq 0.45;\ 0.5\ ppt \leq S \leq 15\ ppt \tag{9}$$

Regression analysis indicates that parameter b is correlated only with salinity (P-value = 0.000; see Figure 10a), while parameter C is associated with both salinity and solid fraction (P-value = 0.000; see Figure 10b). There is no significant linear relationship between the interactive term and parameter b, as indicated by an individual P-value greater than 0.005. However, a significant linear

association exists between the interactive term and parameter C (individual P-value = 0.002), suggesting that the influence of salinity on parameter C varies depending on the solid fraction. Regression analysis resulted in adjusted R^2 values of 0.83 for b and 0.97 for C, with corresponding RMSE of 0.08 and 0.04, respectively. This mathematical description for variations of UWC is based on the experimental data with a volumetric solid fraction range from 14.4% to 58.6% and a salinity range from 0.5 to 15.2 ppt.

Model Performance Evaluation

The proposed semi-empirical models (Eq. 5 and 9) to describe creep rate and unfrozen water content were evaluated by comparing the measured and calculated data (Figure 11). Figure 11a shows the comparison between the measured and calculated minimum strain rate ($\dot{\epsilon_m}$) using Eq. (5). Figure 11b compares the measured and calculated normalized unfrozen water content ($\theta_{n,u}$) using Eq. (9). The 242 measured data points on $\dot{\epsilon_m}$ were collected from this research and previous studies (Bray 2012; Bray 2013) within the tested stress range. The test data can be found in Table S2 in the supplementary materials. The 84 data points on $\theta_{n,u}$ were calculated based on measured gravimetric unfrozen water content summarized in Table 3. The semi-empirical models demonstrate reasonable reproductions of the test data on both $\dot{\epsilon_m}$ and $\theta_{n,u}$. The robust correlations are evidenced by the overall correlation factor (R^2) of 0.9 and 0.88 for $\dot{\epsilon_m}$ and $\theta_{n,u}$, respectively.

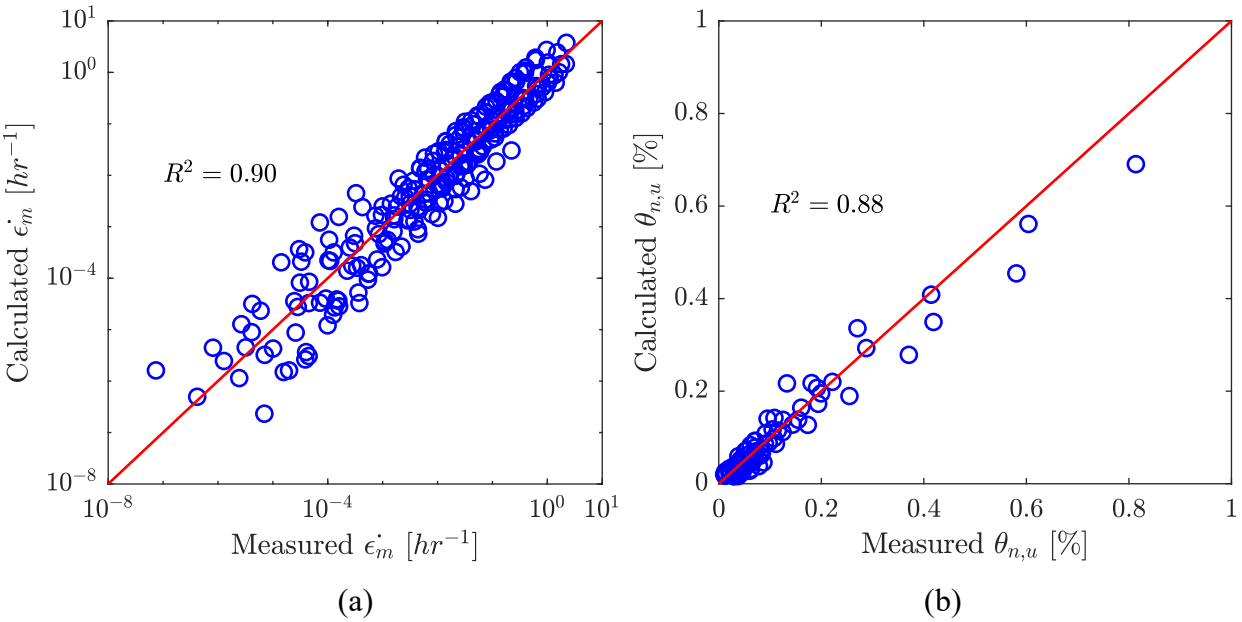

Figure 11. Comparison between the measurements and calculations: (a) minimum strain rate; (b) normalized unfrozen water content.

Interactive Effects of Solid Fraction, Temperature, and Axial Stress

Influence of Temperature on the Effect of Volumetric Solid Fraction

Figure 12 shows the variations of minimum strain rate ($\dot{\epsilon}_m$) with temperature (T), volumetric solid fraction (θ_s), and axial stress (σ_1). Previous empirical evidence suggests an independent effect of volumetric ice content (and therefore volumetric solid fraction) and temperature on $\dot{\epsilon}_m$ in triaxial stress regimes (Arenson and Springman 2005). However, the observations in this study demonstrate competing effects of solid fraction and temperature on $\dot{\epsilon}_m$ under uniaxial stress conditions. The strengthening effect of the increased solid fraction is reduced at warmer temperatures. This diminished strengthening effect is evidenced by the significant increase in $\dot{\epsilon}_m$ with increased temperature in higher solid fractions (Figure 12a) and the lower decreasing rate in $\dot{\epsilon}_m$ with increased volumetric solid fraction at warmer temperatures (Figure 12b). These results highlight the interactive effect of solid fraction and temperature, as the reinforcing effect of

isolated solid particles on the creep deformation of ice-rich permafrost diminishes at higher sub-freezing temperatures. At the same volumetric solid fraction conditions, the effect of temperature on the relationship between $\dot{\epsilon_m}$ and axial stress is constant, with the same increasing rates in $\dot{\epsilon_m}$ at different temperatures (Figure 12c).

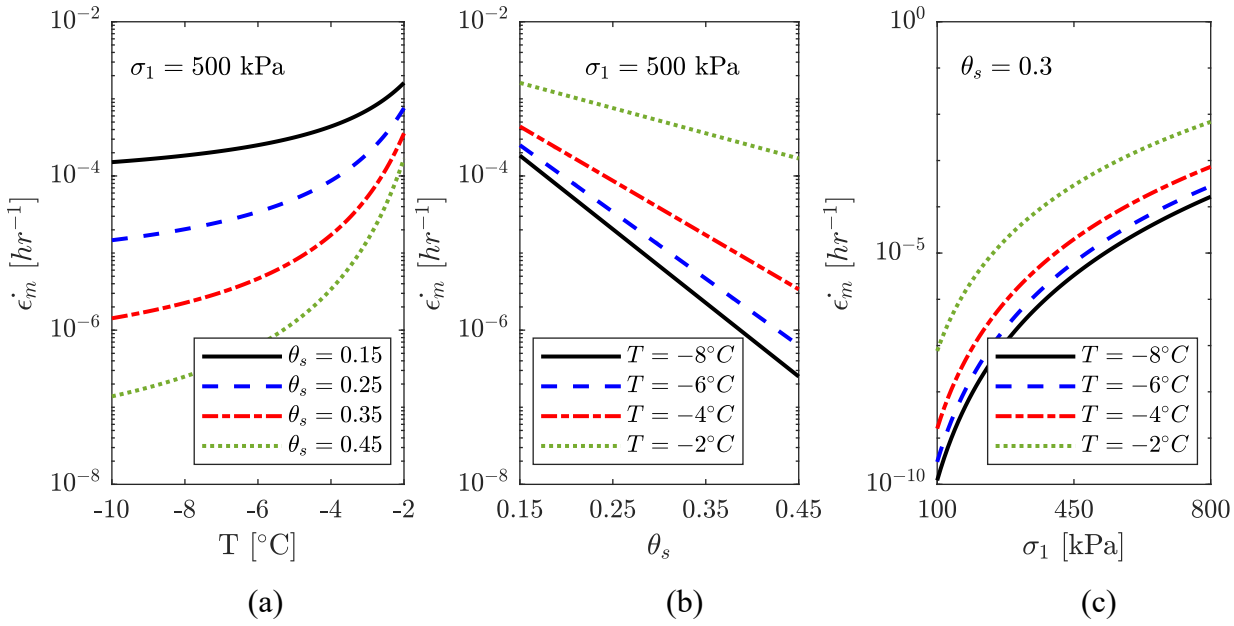

Figure 12. Variations of minimum strain rate as a function of temperature (T), volumetric solid fraction (θ_s), and axial stress (σ_1).

The competing effects of solid fraction and temperature on minimum strain rate may be attributed to the growth of unfrozen water content (Cuffey and Paterson 2010). To quantify the role of unfrozen water content in creep deformation, the established UWC power law model (Eq. 9) was used to investigate the effect of $\theta_{n,u}$ on Glen's flow law parameters A and n, as shown in Figure 13. The discrete points were calculated based on the index properties of the tested samples. The lines were calculated using the empirical relationships between temperature and solid fraction with parameters A, n (Eq. 3 and 4), and C, b (Eq. 7 and 8) at three volumetric solid fractions.

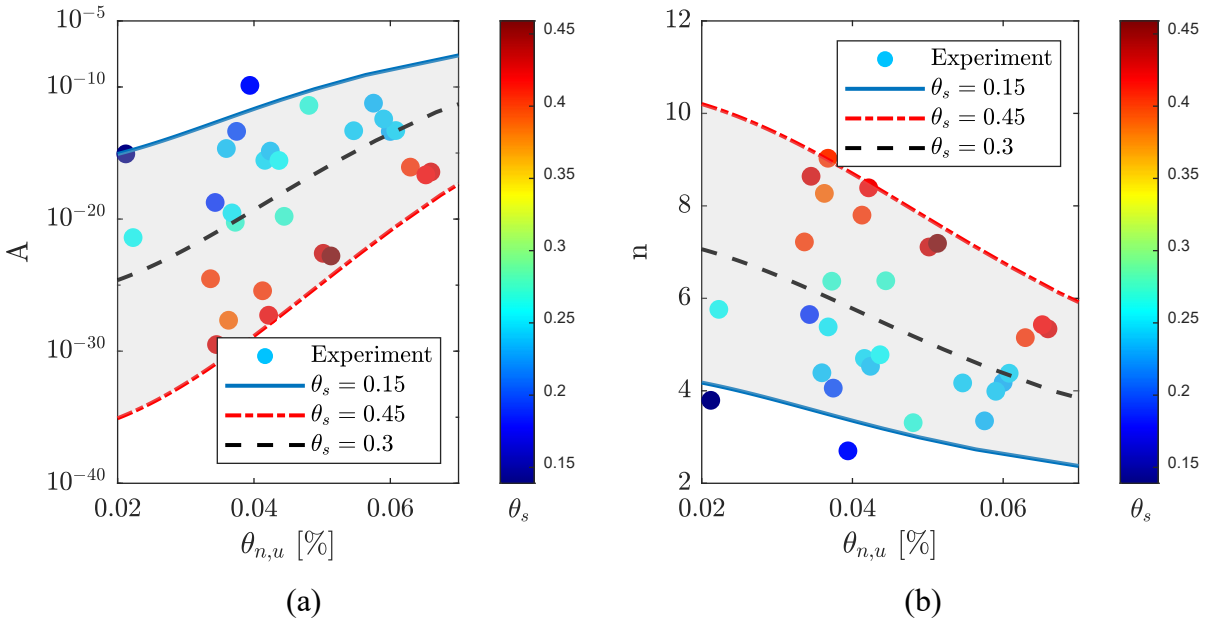

Figure 13. Effect of normalized unfrozen water content on parameters of Glen's flow law at different volumetric solid fractions: (a) parameter A vs. normalized unfrozen water content; (b) parameter n vs. normalized unfrozen water content.

The general trend in Figure 13 suggests that with increasing $\theta_{n,u}$, A increases and n decreases. This trend is more pronounced at higher solid fractions. The increase in A may indicate a reduction in viscosity, as the presence of unfrozen water acts as a lubricant between particles and the ice matrix, facilitating relative displacement. Reduced n indicates a less nonlinear relationship between minimum strain rate and axial stress. This reduced sensitivity of permafrost to axial stress is attributed to the more uniform stress distribution at particle-ice and particle-particle contacts caused by increasing unfrozen water. As shown in Figure 8, the increase of volumetric solid fraction decreases A and increases n. Increased unfrozen water content reduces the effect of solid fraction on creep deformation through facilitating relative displacement and modulating stress distributions at particle-particle and particle-ice contacts. The observed competition between the effects of solid fraction and temperature is thus attributed to these amplified lubricating and modulating effects of unfrozen water content at higher solid fractions. Using Eq. 9, Figures 14a

and 14b depict the variations of $\theta_{n,u}$ with temperature for ice-rich silty permafrost of two salinities, 2 ppt and 15 ppt, respectively. At both salinities, samples with higher solid fractions contain much higher $\theta_{n,u}$ as temperature increases. The elevated $\theta_{n,u}$ is induced by the higher content of fine-grained particles in samples with a higher solid fraction. This elevated $\theta_{n,u}$ weakens the ice matrix and further diminishes the strengthening effect of solid fraction on the creep deformation.

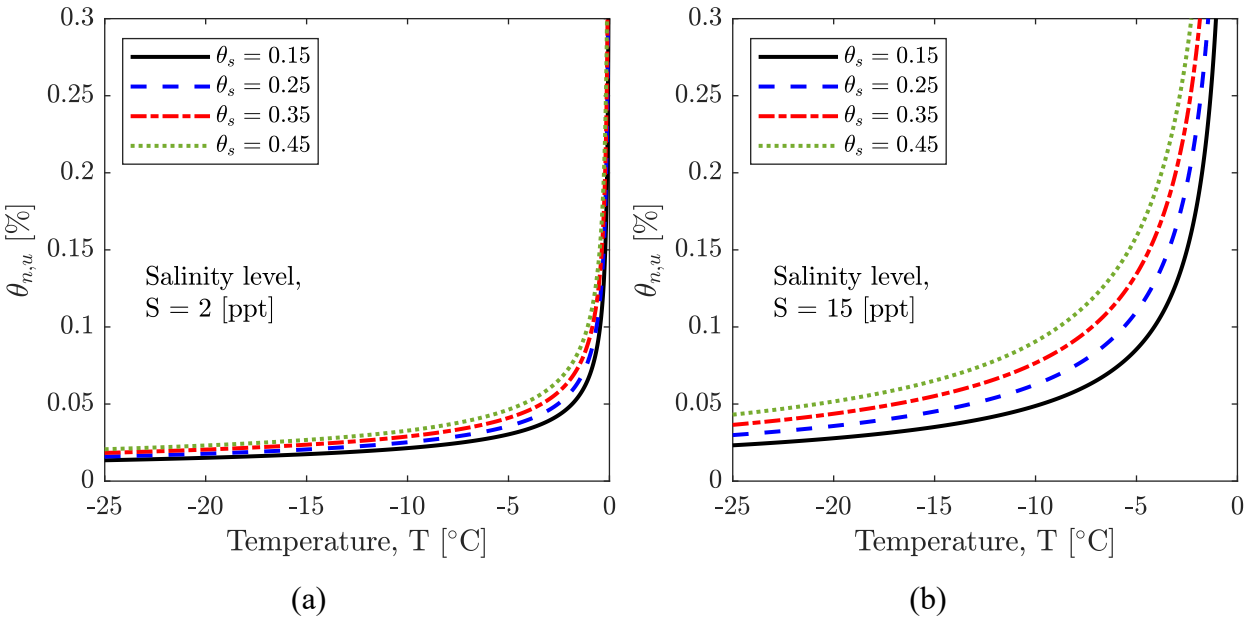

Figure 14. Variations of normalized unfrozen water content: (a) at 2 ppt salinity; (b) at 15 ppt salinity.

Influence of Axial Stress on the Effect of Volumetric Solid Fraction

Moore (2014) concluded that soil particle inclusions could either strengthen or weaken clean ice depending on the applied stress magnitude. Ice containing solid particles becomes weaker than clean ice and exhibits a higher creep rate when the applied stress exceeds a certain stress level. This study reveals that the effect of solid fraction on creep deformation of ice-rich permafrost is influenced by axial stress. Figure 15 shows the variation of minimum strain rate with axial stress

of ice-rich permafrost of two volumetric solid fractions under similar temperatures. Figure 15(a) is based on experimental results by Bray (2013) and Figure 15(b) is based on Eq. 5.

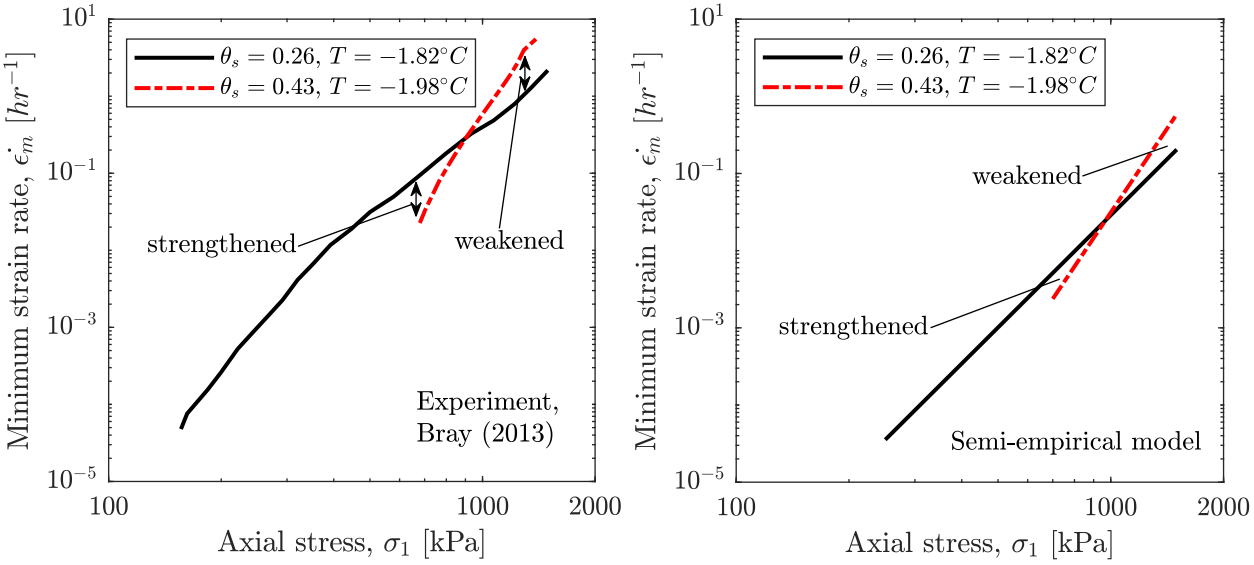

Figure 15. Influence of axial stress on the effect of volumetric solid fraction on minimum strain rate during CSC tests: (a) experimental measurements (Bray 2013); (b) model calculations based on Eq. 5.

Figure 15 shows that at lower axial stress conditions, an increase in volumetric solid fraction strengthens the permafrost by reducing the minimum strain rate. Increasing the volumetric solid fraction increases the number of isolated solid particles that hinder creep deformation, thus decreasing the minimum strain rate. The reinforcing effect of solid particles is evident from the enhanced viscosity (indicated by higher *A* parameters as shown in Figure 8a) at low axial stress. At higher axial stress conditions, an increase in volumetric solid fraction weakens the permafrost by increasing the creep strain rate. This weakening effect of increasing solid fraction on creep deformation is attributed to the increased sensitivity of permafrost to axial stress, evidenced by higher *n* parameters at higher solid fractions (Figure 8b). Permafrost with a higher *n* value shows a strong nonlinear response to axial stress and deforms more rapidly under higher axial stress. This

highly nonlinear relationship between minimum strain rate and axial stress may be caused by the increased susceptibility of the ice matrix to deformation at higher solid fractions. Permafrost may transition from a creep decelerating process to a creep accelerating process at relatively higher axial stresses.

The weakening of permafrost's creep resistance due to an increase in volumetric solid fraction was also observed in the UCS tests at a relatively higher strain rate, as shown in Figure 16. Several experimental studies have shown that the ratio between the peak compressive stress σ_{max} and the constant strain rate $\dot{\epsilon}$ at the UCS tests is approximately equal to the ratio between the constant axial stress σ_1 and the minimum strain rate $\dot{\epsilon}_m$ at the CSC tests (Mellor 1979; Hooke et al. 1980; Ladanyi 1981; Zhu and Carbee 1987; Andersland and Ladanyi 2003; Arenson and Springman 2003). Such correlation is due to the similar material response to the UCS and CSC tests (Arenson and Springman 2005). Figure 16 suggests that at the same minimum strain rate, samples with lower volumetric solid fraction can sustain higher axial stress compared to samples with higher volumetric solid fraction. This observation is consistent with the patterns of the creep response of permafrost samples at relatively high axial stress conditions in Figure 15.

Figure 17 depicts the variations of minimum strain rate of the ice-rich silty permafrost at volumetric solid fractions of 0.15 and 0.45 as a function of temperature and axial stress. Using Eq. 5, the minimum strain rates were calculated within the stress and temperature ranges of the experiments listed in Table 2. The increase in volumetric solid fraction increases the creep resistance, thus decreasing creep rate at lower temperatures and lower axial stresses (*e.g.*, -10°C and 500 kPa). Such a strengthening effect of increasing solid fraction diminishes at warmer

temperatures due to the effect of unfrozen water. The effect of solid fraction reverses at near-melting point temperatures and under higher axial stresses (*e.g.*, -2℃ and 1000 kPa), where an increase in volumetric solid fraction increases the creep rate.

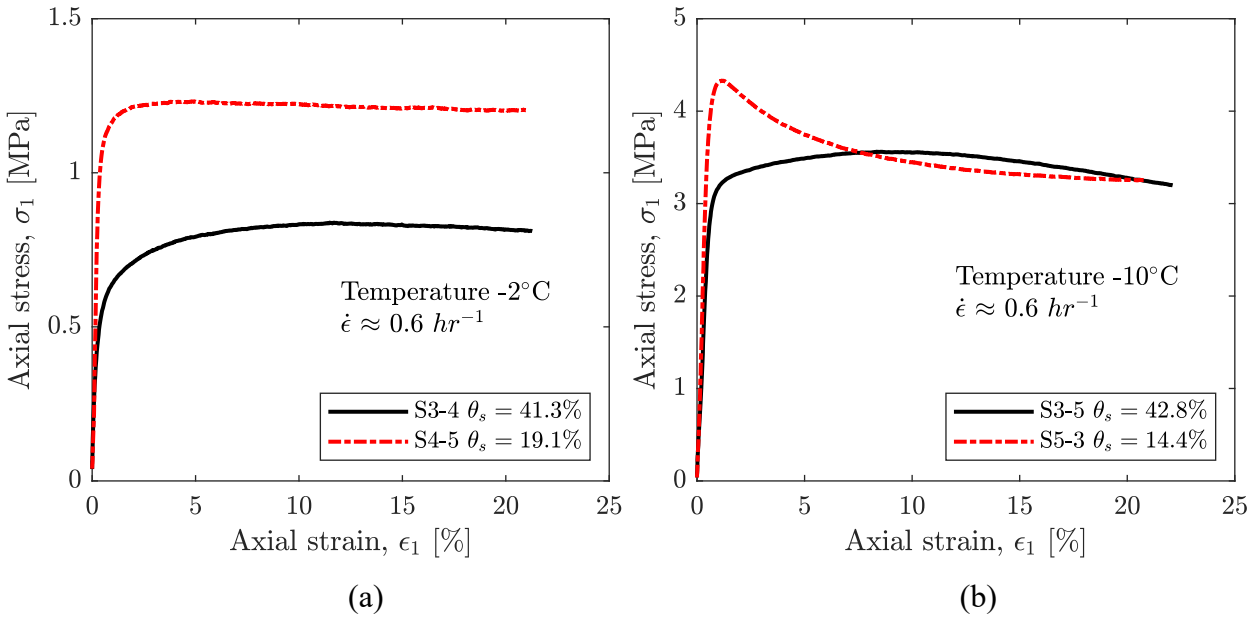

(a) (b)

Figure 16. Effect of volumetric solid fraction on peak compressive strength during UCS tests at a relatively high strain rate of 0.6 hr^{-1}: (a) stress-strain response at -2℃; (b) stress-strain response at -10℃.

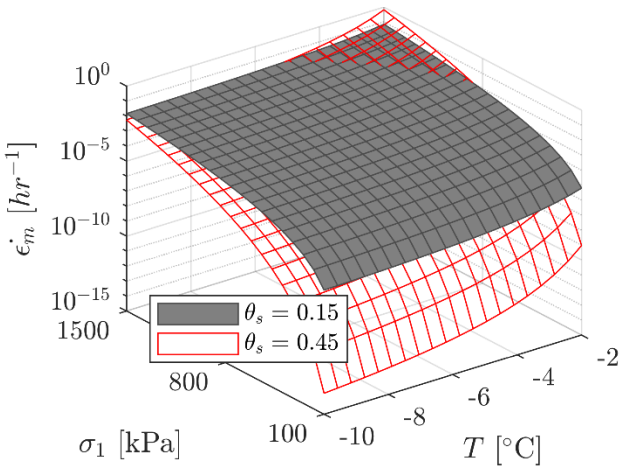

Figure 17. Minimum strain rate as a function of volumetric solid fraction, temperature, and axial stress within the testing range.

Figure 18 shows a conceptual diagram illustrating the mechanism of the interactive effects of solid fraction, temperature, and axial stress on creep deformation of ice-rich silty permafrost at the particle scale. A higher solid fraction hinders creep deformation, enhances viscosity at low axial stress, and decreases the creep rate. As a result, the increase in solid fraction shows a strengthening effect on creep resistance of permafrost at colder temperatures and low axial stresses. The unfrozen water content significantly increases with temperature near the melting point. The increase in unfrozen water content diminishes the strengthening effect of solid fraction and weakens the ice matrix. Therefore, the increase in solid fraction shows a reduced strengthening effect on creep resistance of permafrost at warmer temperatures and low axial stresses. At warmer temperatures and higher axial stresses, a higher solid fraction leads to a highly nonlinear response to axial stress, wherein the minimum strain rate increases drastically with higher axial stress. The combined effect of increased axial stress and unfrozen water content results in the formation and growth of cracks and the weakening effect of increasing solid fraction.

Limitations of This Study

The data, equations, and discussion presented in this paper are based on limited laboratory results for ice-rich silty permafrost under uniaxial stress conditions. The mathematical relationships between secondary creep rate and volumetric solid fraction, temperature, and axial stress presented in this study can reproduce the test data to a certain extent. However, further experimental, analytical, and numerical studies are recommended to investigate the proposed mechanisms and relationships. Several uncertainties should be expected during the interpretation of the observed mechanisms. First, the creep response of permafrost is influenced by the distribution and orientation of ice. The heterogeneous distribution of ice in permafrost can lead to high variability

in the results. Second, the semi-empirical model (Eq. 5) that calculates the minimum strain rate should be used cautiously, especially at low axial stress (<150 kPa), as the minimum creep rate might not be reached at low axial stress during the laboratory test durations. Third, the test data and model were based on saturated permafrost sampled from the Arctic Coastal Plain. However, presence of air in permafrost can affect its creep mechanism by influencing the ice structure, pore pressure, and temperature variations.

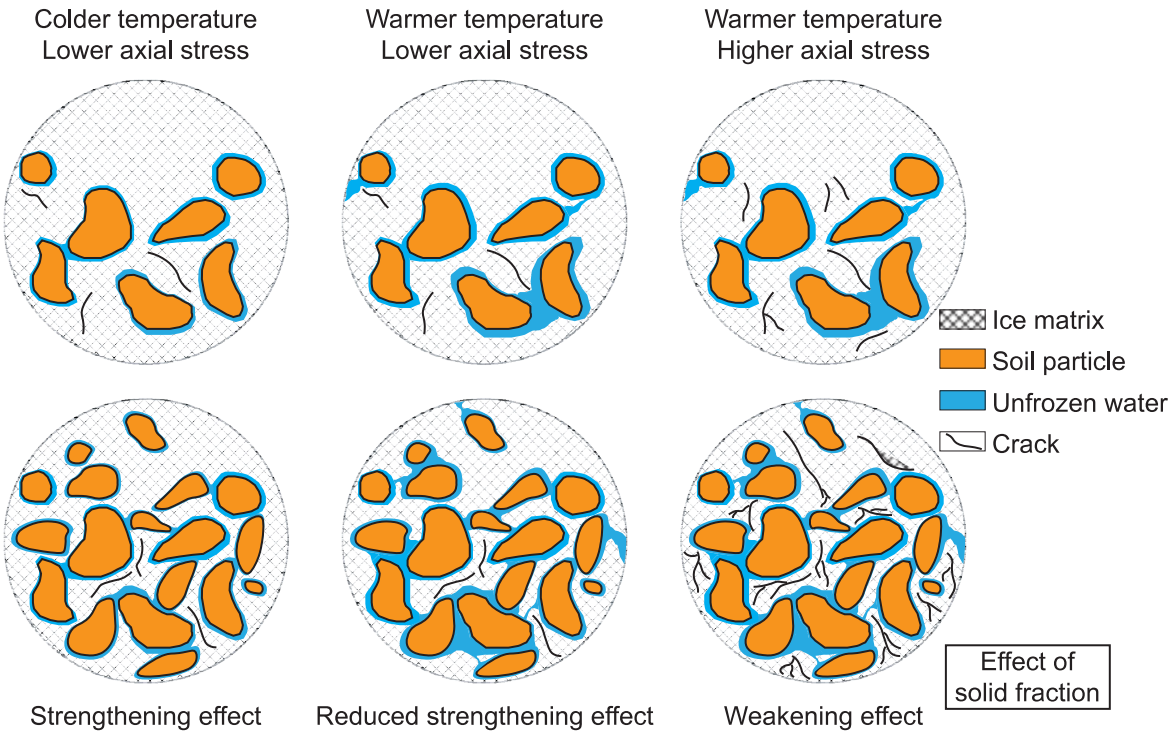

Figure 18. Conceptual diagram illustrating the particle-scale mechanism of the interactive effects of volumetric solid fraction, temperature, and axial stress on creep deformation.

Summary and Conclusions

The objective of this paper is to quantitatively assess the effect of volumetric solid fraction on the creep deformation of ice-rich silty permafrost and to analyze factors that may interactively influence the solid fraction effect, including temperature and axial stress. A geotechnical

investigation of near-surface permafrost soils (upper 1.5 m) sampled near Utqiaġvik, Alaska was first carried out for geotechnical characterization. The experimental approach included constant strain rate creep tests, unconfined compressive tests, and unfrozen water content tests. Mathematical descriptions of the experimental data were established to quantify the creep deformation behavior of ice-rich silty permafrost. This research leads to the following key conclusions:

- The permafrost at shallow depth in the tundra near Utqiaġvik, Alaska is predominantly ice-rich with ataxitic cryostructure and non-uniformly distributed ice.
- The increase in volumetric solid fraction can either increase or decrease the creep resistance of ice-rich silty permafrost. The effect of volumetric solid fraction on creep also depends on temperature and axial stress.
- At lower temperatures and lower axial stresses (*e.g.*, -10℃ and 500 kPa), the increase in solid fraction strengthens the creep resistance. This strengthening effect may be caused by the hindered creep deformation and enhanced viscosity at low axial stress by an increased solid fraction.
- The increase in solid fraction has a reduced strengthening effect on creep resistance of permafrost at warmer temperatures and low axial stresses. This reduction is attributed to the increase in unfrozen water content. An increase in unfrozen water content diminishes the strengthening effect of solid fraction on creep deformation of ice-rich permafrost. This diminishing effect caused by unfrozen water content is amplified at higher solid fractions. In addition, silty permafrost with higher volumetric solid fraction contains higher unfrozen water content; higher unfrozen water content weakens the ice matrix and further diminishes the strengthening effect of solid fraction on the creep deformation.

- At warmer temperatures near the melting point and higher axial stresses (*e.g.*, -2℃ and 1000 kPa), the increase in solid fraction reduces the creep resistance, resulting in an increasing creep rate. This weakening effect is attributed to the highly nonlinear relationship between minimum strain rate and axial stress of permafrost at higher solid fractions, where minimum strain rate increases drastically with higher axial stress. The combined effect of increased axial stress and unfrozen water results in the weakening effect of increasing solid fraction.

Data availability statement: Some or all data, models, or code that support the findings of this study are available from the corresponding author upon request.

Acknowledgements: Z.W., M.X., J.H. were supported by the U.S. National Science Foundation (NSF) (grant number: RISE-1927718). M.X. was also supported by NSF (grant numbers: OISE-1927137, OPP-1945369).

References

Andersland, O.B. and Ladanyi, B., 2003. *Frozen ground engineering*. John Wiley & Sons.

Anderson, D.M. and Morgenstern, N.R., 1973, July. Physics, chemistry and mechanics of frozen ground: A review. In *Proceedings of the Second International Conference on Permafrost* (pp. 257-288). National Academy of Sciences Washington, DC.

Anderson, D.M. and Tice, A.R., 1973. The unfrozen interfacial phase in frozen soil water systems. In *Physical aspects of soil water and salts in ecosystems* (pp. 107-124). Berlin, Heidelberg: Springer Berlin Heidelberg.

Anisimov, O.A. and Nelson, F.E., 1996. Permafrost distribution in the Northern Hemisphere under scenarios of climatic change. *Global and Planetary Change*, 14(1-2), pp.59-72.

Arenson, L.U. and Springman, S.M., 2005. Mathematical descriptions for the behaviour of ice-rich frozen soils at temperatures close to 0 C. *Canadian Geotechnical Journal, 42*(2), pp.431-442.

Arenson, L.U., Johansen, M.M. and Springman, S.M., 2004. Effects of volumetric ice content and strain rate on shear strength under triaxial conditions for frozen soil samples. *Permafrost and Periglacial Processes, 15*(3), pp.261-271.

ASTM Int'l, 2006. *Standard Test Method for Laboratory Determination of Strength Properties of Frozen Soil at a Constant Rate of Strain*. D 7300 – 06.

ASTM Int'l, 2006. *Standard Test Method for Sieve Analysis of Fine and Coarse Aggregates*, C 136.

ASTM Int'l, 2007. *Standard Test Method for Particle-Size Analysis of Soils*, D 422 – 63.

ASTM Int'l, 2017. *Standard test methods for liquid limit, plastic limit, and plasticity index of soils*. D4318-17e1.

Biskaborn, B.K., Smith, S.L., Noetzli, J., Matthes, H., Vieira, G., Streletskiy, D.A., Schoeneich, P., Romanovsky, V.E., Lewkowicz, A.G., Abramov, A. and Allard, M., 2019. Permafrost is warming at a global scale. *Nature communications, 10*(1), p.264.

Bray, M.T., 2012. The influence of cryostructure on the creep behavior of ice-rich permafrost. *Cold regions science and technology, 79*, pp.43-52.

Bray, M.T., 2013. Secondary creep approximations of ice-rich soils and ice using transient relaxation tests. *Cold regions science and technology, 88*, pp.17-36.

Chuvilin, E., Sokolova, N. and Bukhanov, B., 2022. Changes in Unfrozen Water Contents in Warming Permafrost Soils. *Geosciences*, *12*(6), p.253.

Clarke, E.S. ed., 2007, September. Permafrost foundation: state of the practice. American Society of Civil Engineers.

Cudmani, R., Yan, W. and Schindler, U., 2022. A constitutive model for the simulation of temperature-, stress-and rate-dependent behaviour of frozen granular soils. *Géotechnique*, pp.1-13.

Cuffey, K.M. and Paterson, W.S.B., 2010. *The physics of glaciers*. Academic Press.

Dash, J.G., Rempel, A.W. and Wettlaufer, J.S., 2006. The physics of premelted ice and its geophysical consequences. *Reviews of modern physics*, *78*(3), p.695.

Dou, S., Nakagawa, S., Dreger, D. and Ajo-Franklin, J., 2016. A rock-physics investigation of unconsolidated saline permafrost: P-wave properties from laboratory ultrasonic measurements. *Geophysics, 81*(1), pp.WA233-WA245.

Duval, P., 1977. The role of the water content on the creep rate of polycrystalline ice.

Glen, J.W., 1955. The creep of polycrystalline ice. *Proceedings of the Royal Society of London. Series A. Mathematical and Physical Sciences, 228*(1175), pp.519-538.

Hivon, E. and Sego, D.C., 1990, June. Determination of the unfrozen water content of saline permafrost using time-domain reflectometry (TDR). In *Proceedings of the 5th Canadian Permafrost Conference* (pp. 257-262). Quebec City, Quebec, Canada: Univ. Laval.

Hjort, J., Streletskiy, D., Doré, G., Wu, Q., Bjella, K. and Luoto, M., 2022. Impacts of permafrost degradation on infrastructure. *Nature Reviews Earth & Environment, 3*(1), pp.24-38.

Hooke, R.L., Mellor, M., Budd, W.F., Glen, J.W., Higashi, A., Jacka, T.H., Jones, S.J., Lile, R.C., Martin, R.T., Meier, M.F. and Russell-Head, D.S., 1980. Mechanical properties of polycrystalline ice: An assessment of current knowledge and priorities for research: Report prepared for the International Commission on Snow and Ice, with support from the US National Science Foundation. *Cold Regions Science and Technology, 3*(4), pp.263-275.

ISO, D., 1994. Soil Quality. Determination of the Specific Electrical Conductivity.

Kanevskiy, M., Shur, Y., Jorgenson, M.T., Ping, C.L., Michaelson, G.J., Fortier, D., Stephani, E., Dillon, M. and Tumskoy, V., 2013. Ground ice in the upper permafrost of the Beaufort Sea coast of Alaska. *Cold Regions Science and Technology, 85,* pp.56-70.

Konrad, J.M., 1990. Segregation potential–pressure–salinity relationships near thermal steady state for a clayey silt. *Canadian Geotechnical Journal*, *27*(2), pp.203-215.

Kruse, A.M., Darrow, M.M. and Akagawa, S., 2018. Improvements in measuring unfrozen water in frozen soils using the pulsed nuclear magnetic resonance method. *Journal of Cold Regions Engineering, 32*(1), p.04017016.

Ladanyi, B. and Morel, J.F., 1990. Effect of internal confinement on compression strength of frozen sand. *Canadian Geotechnical Journal, 27*(1), pp.8-18.

Ladanyi, B., 1972. An engineering theory of creep of frozen soils. *Canadian Geotechnical Journal, 9*(1), pp.63-80.

McFadden, T.T., 2001. *Design Manual for Stabilizing Foundations on Permafrost.* Permafrost Technology Foundation. https://cchrc.org/media/DesignManualforStabilizingFoundationsonPermafrost.pdf

Moore, P.L., 2014. Deformation of debris‐ice mixtures. *Reviews of Geophysics, 52*(3), pp.435-467.

Morgenstern, N.R., Roggensack, W.D. and Weaver, J.S., 1980. The behaviour of friction piles in ice and ice-rich soils. *Canadian Geotechnical Journal, 17*(3), pp.405-415.

Nixon, J.F. and Lem, G., 1984. Creep and strength testing of frozen saline fine-grained soils. *Canadian geotechnical journal, 21*(3), pp.518-529.

Nixon, J.F. and McRoberts, E.C., 1976. A design approach for pile foundations in permafrost. *Canadian Geotechnical Journal, 13*(1), pp.40-57.

Orth, W., 1988. A creep formula for practical application based on crystal mechanics. In *Proc. 5th Int. Symp. on Ground Freezing, Nottingham, England, ed. RH Jones and JT Holden. Rotterdam: A. A. Balkema* (Vol. 1, pp. 205-11).

Rantanen, M., Karpechko, A.Y., Lipponen, A., Nordling, K., Hyvärinen, O., Ruosteenoja, K., Vihma, T. and Laaksonen, A., 2022. The Arctic has warmed nearly four times faster than the globe since 1979. *Communications Earth & Environment, 3*(1), p.168.

Sayles, F.H. and Haines, D., 1974a. Creep of frozen silt and clay (No. 252). Corps of Engineers, US Army, Cold Regions Research and Engineering Laboratory.

Sayles, F.H., 1974b. *Triaxial constant strain rate tests and triaxial creep tests on frozen Ottawa sand* (No. 253). Corps of Engineers, US Army Cold Regions Research and Engineering Laboratory.

Schindler, U., Cudmani, R., Chrisopoulos, S. and Schünemann, A., 2023. Multi-stage creep behavior of frozen granular soils: Experimental evidence and constitutive modeling. *Canadian Geotechnical Journal*, (ja).

Shastri, A., Sánchez, M., Gai, X., Lee, M.Y. and Dewers, T., 2021. Mechanical behavior of frozen soils: Experimental investigation and numerical modeling. *Computers and Geotechnics, 138*, p.104361.

Shelman, A., Tantalla, J., Sritharan, S., Nikolaou, S. and Lacy, H., 2014. Characterization of seasonally frozen soils for seismic design of foundations. *Journal of Geotechnical and Geoenvironmental Engineering, 140*(7), p.04014031.

Swinzow, G.K., 1962. Investigation of shear zones in the ice sheet margin, Thule area, Greenland. *Journal of Glaciology, 4*(32), pp.215-229.

Ting, J.M., Torrence Martin, R. and Ladd, C.C., 1983. Mechanisms of strength for frozen sand. *Journal of Geotechnical Engineering, 109*(10), pp.1286-1302.

Vialov, S.S., 1965. Rheological properties and bearing capacity of frozen soils.

Voitkovskii, K.F., 1960. The mechanical properties of ice. Bedford, MA: Air Force Cambridge Research Laboratories, Geophysics Research Directorate.

Vyalov, S.S., 2013. *Rheological fundamentals of soil mechanics*. Elsevier.

Wang, J., Zhang, F., Yang, Z.J. and Yang, P., 2022. Experimental investigation on the mechanical properties of thawed deep permafrost from the Kuparuk River Delta of the North Slope of Alaska. *Cold Regions Science and Technology, 195*, p.103482.

Wang, Z., Xiao, M., Liew, M., Jensen, A., Farquharson, L., Romanovsky, V., Nicolsky, D., McComb, C., Jones, B.M., Zhang, X. and Alessa, L., 2023a. Arctic geohazard mapping tools for civil infrastructure planning: a systematic review. *Cold Regions Science and Technology*, p.103969.

Wang, Z., Xiao, M., Nicolsky, D., Romanovsky, V., McComb, C. and Farquharson, L., 2023b. Arctic coastal hazard assessment considering permafrost thaw subsidence, coastal erosion, and flooding. *Environmental Research Letters, 18*(10), p.104003.

Watanabe, K. and Wake, T., 2009. Measurement of unfrozen water content and relative permittivity of frozen unsaturated soil using NMR and TDR. *Cold Regions Science and Technology, 59*(1), pp.34-41.

Weaver, J.S. and Morgenstern, N.R., 1981. Pile design in permafrost. *Canadian geotechnical journal, 18*(3), pp.357-370.

Yang, Z.J., Still, B. and Ge, X., 2015. Mechanical properties of seasonally frozen and permafrost soils at high strain rate. *Cold regions science and technology, 113*, pp.12-19.

Zhu, Y. and Carbee, D.L., 1984. Uniaxial compressive strength of frozen silt under constant deformation rates. *Cold regions science and technology, 9*(1), pp.3-15.